CHEMISTRY

Constraint of a ruthenium-carbon triple bond to a five-membered ring

Qingde Zhuo*, Hong Zhang*, Yuhui Hua, Huijun Kang, Xiaoxi Zhou, Xinlei Lin, Zhixin Chen, Jianfeng Lin, Kaiyue Zhuo, Haiping Xia†

The incorporation of a metal-carbon triple bond into a ring system is challenging because of the linear nature of triple bonds. To date, the synthesis of these complexes has been limited to those containing third-row transition metal centers, namely, osmium and rhenium. We report the synthesis and full characterization of the first cyclic metal carbyne complex with a second-row transition metal center, ruthenapentalyne. It shows a bond angle of 130.2(3)° around the sp-hybridized carbyne carbon, which represents the recorded smallest angle of second-row transition metal carbyne complexes, as it deviates nearly 50° from the original angle (180°). Density functional theory calculations suggest that the inherent aromatic nature of these metallacycles with bent Ru≡C–C moieties enhances their stability. Reactivity studies showed striking observations, such as ambiphilic reactivity, a metal-carbon triple bond shift, and a [2 + 2] cycloaddition reaction with alkyne and cascade cyclization reactions with ambident nucleophiles.

INTRODUCTION

Transition metal complexes containing metal-carbon triple bonds (namely, metal carbyne or metal alkylidyne complexes) hold an important place in chemistry because they stimulate fundamental investigations of metal-carbon interactions and are valuable in synthetic chemistry as homogeneous catalysts or precursors for interesting organometallic compounds (*1*–*4*). Accordingly, the chemistry of the metal-carbon triple bond has been an area of intense interest and has attracted tremendous attention in both industry and academia since the seminal work by Fischer *et al.* (*5*). Although a wide variety of metal carbyne complexes are known, most documented examples feature acyclic structures. The linear geometry of the sp-hybridized carbyne carbon makes the synthesis of cyclic metal carbyne complexes particularly difficult. Thus, cyclic metal carbyne complexes remained elusive until the pioneering works by Wen *et al.* (*6*) (Fig. 1). Until now, well-defined cyclic metal carbynes were only known for third-row transition metal centers osmium and rhenium, namely, osmabenzynes (*7*–*9*), rhenabenzynes (*10*), osmapyridynes (*11*), osmapentalynes (*12*, *13*), and dirhenadehydro[12]annulenes (*14*), whereas these complexes with non–third-row transition metals have not yet been accomplished.

The lack of non–third-row transition metal carbynes is not surprising. Traditionally, the strength of transition metal–carbon bonds decreases with the ascending of a column in the periodic table (*15*), which results in relative lability of the first- and second-row organometallic compounds in comparison with their third-row analogs (*16*, *17*). In particular, cyclic metal carbyne complexes with first- and second-row transition metals are considerably less stable than their third-row counterparts both thermodynamically and kinetically, as demonstrated by computational analysis (*18*, *19*). Thus, intrinsic instability of the non–third-row transition metal carbynes is responsible for their absence, which greatly restrained their synthesis and further exploration.

During our recent studies on the chemistry of metallacyclic complexes, we found that typically unstable species could show enhanced stability owing to metalla-aromaticity, which yielded a number of exceptional organometallic complexes with osmium and ruthenium centers (*12*, *20*, *21*). These results prompted us to explore the construction of cyclic metal carbyne complexes with second-row transition metal centers using our synthetic strategies for metalla-aromatics. Herein, we report the synthesis and characterization of unprecedented ruthenium-based cyclic carbyne complexes, that is, ruthenapentalynes. These ruthenapentalynes exhibit good stability in the solid state, although the bent Ru≡C–C moiety shows a bond angle of only 130.2(3)°, which deviates considerably from the linear nature of the sp-hybridized carbyne carbon. Experimental and computational studies revealed the inherent aromaticity of these cyclic ruthenium carbyne complexes. Synergistic interplay of aromaticity and ring strain results in the unique reactivities of ruthenapentalyne, providing access to a series of novel polycyclic aromatic molecules with a second-row transition metal.

RESULTS

Synthesis and characterization of ruthenapentalynes

We recently established an efficient aromaticity-driven method for the construction of cyclic osmium carbyne complexes based on multiyne chains (termed carbolongs) (*13*). We envisioned that the powerful ligating ability of carbolongs would lead to the realization of cyclic metal carbyne complexes with second-row transition metal centers. As shown in Fig. 2A, we formed the expected cyclic ruthenium carbyne complex **2a** and isolated it as a red solid in 65% yield when a solution of carbolong **1a** was treated with $RuCl_2(PPh_3)_3$ and excess PPh_3 at room temperature (RT) for 3 hours. We also obtained a similar cyclic ruthenium carbyne complex, **2b**, upon reacting **1b** with $RuCl_2(PPh_3)_3$.

High-resolution mass spectrometry (HRMS), elemental analysis (EA), and nuclear magnetic resonance (NMR) spectroscopy supported the identification of **2a** and **2b**. In the ^{1}H NMR spectrum, we observed the two resonances from the metallacyclic skeletons at 13.06 and 7.32 parts per million (ppm) (**2a**) and 13.17 and 7.35 ppm (**2b**), which are located in the metalla-aromatic region and are comparable to those of osmapentalynes (*12*, *13*). The ^{13}C NMR spectrum exhibits characteristic low-field signals at 355.69 (**2a**) and 355.57 (**2b**) ppm for the carbyne carbons, which are comparable to the signals of previously reported ruthenium carbyne complexes (*22*, *23*). However, these

State Key Laboratory of Physical Chemistry of Solid Surfaces, Collaborative Innovation Center of Chemistry for Energy Materials, College of Chemistry and Chemical Engineering, Xiamen University, Xiamen 361005, China.
*These authors contributed equally to this work.
†Corresponding author. Email: hpxia@xmu.edu.cn

chemical shifts are significantly low field–shifted in comparison to those of sp-hybridized carbon atoms in closely related complexes, such as cyclic metal vinylidene complexes (*24*) and cyclic allenes and their metal complexes reported by Bertrand and colleagues (*25*, *26*).

Single-crystal x-ray diffraction analysis determined the solid-state structure of **2a** (Fig. 2B). The structure of **2a** contains two fused five-membered metallacycles with good planarity, as reflected by the small mean deviation (0.015 Å) from the least-squares plane through Ru and C1–C7. The carbon-carbon bond distances within the metallacycles [1.360(7) to 1.412(6) Å] lie between typical single- and double-bond distances. The corresponding carbon-carbon bond lengths, together with the planarity of the metallabicycle, indicate extensive electronic delocalization within the ruthenapentalyne ring in **2a**. Consistent with other cyclic metal carbyne complexes (*6*–*13*), ruthenapentalyne **2a** could be represented by two resonance structures, namely, **2A** with a Ru≡C unit and **2B** with a Ru=C=C unit (Fig. 2A). Because of the extensive electronic delocalization within the metallacycles, as well as the ring strain of small-sized cyclic metal carbyne, the Ru–C1 bond length [1.833(4) Å] in **2a** is longer than those of terminal ruthenium carbynes (1.660 to 1.766 Å) (bond length ranges in this article are all based on a search of the Cambridge Structural Database, version 5.39 in November 2017), whereas it is comparable to the Os≡C triple bond length of the first osmabenzyne [1.815(4) Å] (*6*) and osmapentalyne [1.845(3) Å] (*12*) with aromaticity. The comparability of Os≡C and Ru≡C bond lengths within similar overall structures is explained by the similar atom radii of ruthenium (1.34 Å) and osmium (1.35 Å) atoms (*27*) and exemplified by the identical metal-carbon triple bond lengths of cationic carbyne complex $[Cp^*(PEt_3)_2Ru{\equiv}CCH{=}CPh_2]^{2+}$ (1.765 Å) (*28*) and $[Cp(P^iPr_3)_2Os{\equiv}CCH{=}CPh_2]^{2+}$ (1.764 Å) (*29*). The Ru–C4 [2.104(4) Å] and Ru–C7 [2.036(4) Å] bond distances in **2a** are within the range of the distances of typical Ru–C(vinyl) bonds (1.973 to 2.202 Å), with the Ru–C7 bond length slightly shorter than that of Ru–C4. Notably, the bond angle at the sp-hybridized carbon atom in **2a** is only 130.2(3)°, which, to the best of our knowledge, is far smaller than the previously reported smallest bond angle for a carbyne carbon bonded with a second-row transition metal [152.3(3)°] (*30*). Thus, ruthenapentalyne **2a** can be regarded as the first example of a cyclic metal carbyne complex with a second-row transition metal center, and its exceptional bond angle is the smallest on record for second-row transition metal carbyne complexes.

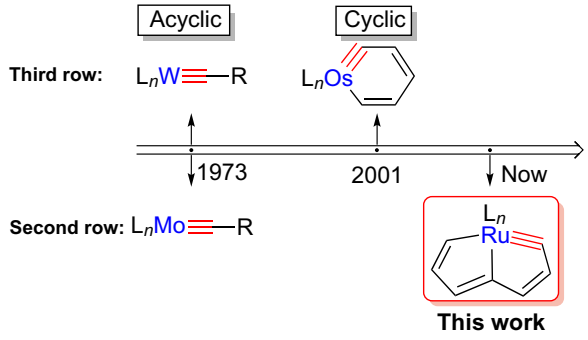

Fig. 1. Development of transition metal carbyne complexes. L, ligand.

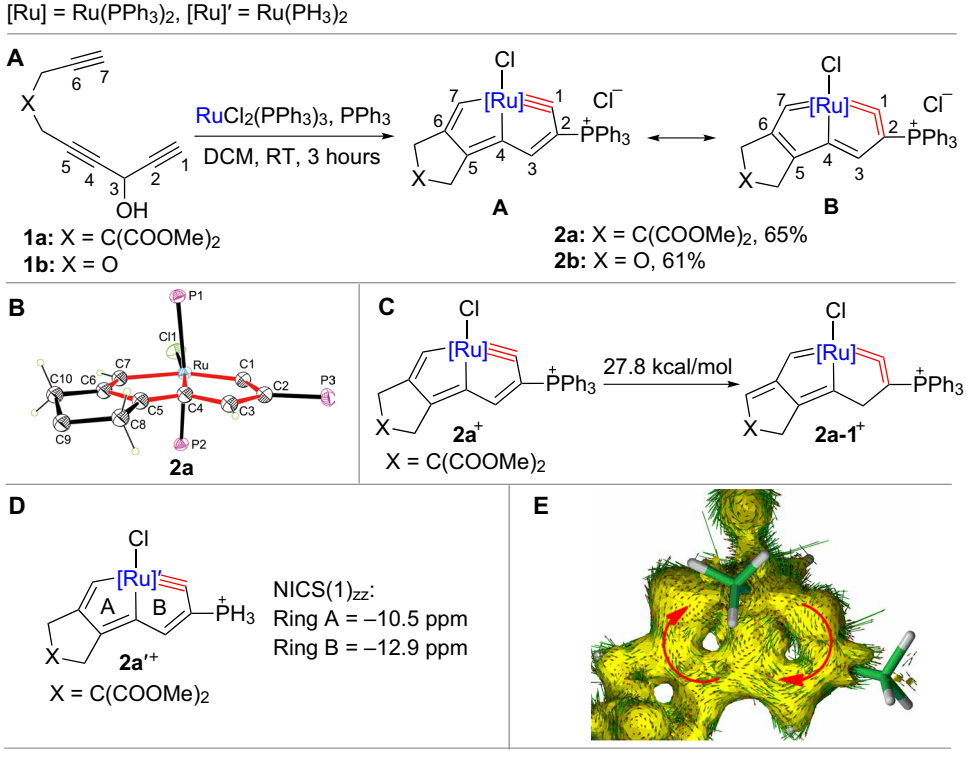

Fig. 2. The synthesis, structure, and aromaticity of ruthenapentalynes 2. (**A**) Synthesis of ruthenapentalynes **2** from carbolongs **1**. DCM, dichloromethane. (**B**) X-ray molecular structure for the cation of ruthenapentalyne **2a** (the ellipsoids are drawn at the 50% probability level; phenyl groups and ester groups are omitted for clarity; the detailed structure is presented in fig. S1). (**C**) ASE evaluation of the aromaticity of ruthenapentalyne **2a**. (**D**) Nucleus-independent chemical shift (NICS)$(1)_{zz}$ evaluations of aromaticity of model complex **2a**′. (**E**) AICD plot of model complex **2a**′ with an isosurface value of 0.03. The magnetic field vector is orthogonal to the ring plane and points upward (aromatic species exhibit clockwise diatropic circulations).

Evaluation of the aromaticity of ruthenapentalyne 2a by density functional theory calculations

Formation of small rings containing sp-hybridized carbon atoms is often disfavored because of strain. However, in this case, ruthenapentalyne **2a** exhibits good thermal stability (the solid sample is persistent in air at 60°C for at least 3 hours). We surmised that the inherent aromaticity of **2a** significantly enhances the stabilization of the five-membered ring with the Ru≡C unit. We performed density functional theory (DFT) computations to evaluate the aromaticity of ruthenapentalyne **2a**. As shown in Fig. 2C, the aromatic stabilization energy (ASE) of **2a** (27.8 kcal/mol) is comparable to those of other reported metalla-aromatics (*31*). We also calculated the nucleus-independent chemical shift along the *z* axis at 1 Å above the ring critical point [$NICS(1)_{zz}$] (*32*) (we used the average value when the environments above and below the ring centers were not equivalent) of model compound **2a′**, which was simplified by replacing the PPh_3 groups with PH_3 groups (Fig. 2D). Both the considerable ASE value and negative nucleus-independent chemical shift (NICS) values suggest that the metallacycles in ruthenapentalyne **2a** are aromatic. In addition, the anisotropy of the induced current density (AICD) analysis confirmed the aromaticity of **2a** (*33*). The obvious diatropic ring current (clockwise vectors) demonstrated the aromatic character, within the metallabicyclic moiety of model ruthenapentalyne **2a′** (Fig. 2E).

Considering the tremendous progress in metalla-aromatic chemistry, it is quite peculiar that a great number of metalla-aromatic species contain third-row transition metals (*34*), whereas only a few of them contain first- and second-row transition metal centers (*35*–*39*). Ruthenapentalyne **2a** represents an important complement to the metalla-aromatic family and distinguishes itself by furnishing a ruthenium carbyne moiety within a five-membered ring. We also conducted DFT calculations to elucidate the formation of ruthenapentalyne **2a** (fig. S7). The computed free-energy profile of the reaction shows that the stability of aromatic ruthenapentalyne is crucial for the overall reaction, which can be classified as an aromaticity-driven process.

Ambiphilic reactivity and [2 + 2] cycloaddition reactions with alkynes

Although ruthenapentalynes **2** are stable in the solid state, the metal carbyne moieties of **2** are highly reactive toward both nucleophiles and electrophiles in solution. As shown in Fig. 3A, the reaction of **2** with sodium thiophenoxide under an atmosphere of CO led to the formation of the nucleophilic addition product ruthenapentalenes **3**, which were characterized by NMR spectroscopy. The ^{1}H NMR spectra showed signals for the metallacycles at 10.87 and 7.83 ppm for **3a** and 10.92 and 7.67 ppm for **3b**. All the NMR shifts are in the typical region for metalla-aromatics, illustrating the aromaticity of **3**. Single-crystal x-ray analysis confirmed the structure of **3b** and disclosed the electronic delocalization within the metallacycles (Fig. 3B). The crystal structure revealed the planarity of the metallabicycles (the mean deviation from the least-squares plane of Ru and C1–C7 is 0.033 Å). The bond lengths of Ru–C1 [2.089(3) Å] and Ru–C7 [2.087(3) Å] are identical, both of them falling within the same range as those of previous reported ruthenabenzenes (1.910 to 2.110 Å) (*20*, *36*). Complexes **3** also show good stability toward air, water, and heat. We evaluated the aromaticity of **3** using DFT calculations (figs. S9 to S11). Despite the great recent interest in such aromatic species, the metallapentalene examples reported are limited to only osmapentalenes (*21*). The synthesis of **3** demonstrates that the incorporation of metals other than osmium into pentalene rings is feasible.

Ruthenapentalynes are also capable of reacting with copper(I) halides. As shown in Fig. 3A, ruthenapentalynes **2** readily reacted with CuCl to afford bimetallic complexes **4**, which were isolated in moderate yield (**4a**, 87%; **4b**, 81%). The NMR spectra and solid-state structure established **4** as bimetallacyclopropene derivatives. Taking **4a** as an example, the C^7H and C^3H signals observed at 13.01 and 7.54 ppm compare well with those in the ^{1}H NMR spectroscopy of the parent complex **2a** (13.06 and 7.32 ppm), whereas the resonance of C^1 (325.76 ppm) is significantly upshifted in comparison with that of **2a** (355.69 ppm), as determined by ^{13}C NMR spectroscopy. We also characterized complex **4a** using single-crystal x-ray diffraction (Fig. 3C). The Ru–C1 bond length [1.907(2) Å] is 0.074 Å longer than that in the parent complex **2a** [1.833(4) Å], and the Ru–Cu1 bond length of 2.5333(4) Å is shorter than the sum of the covalent radii of Ru and Cu atoms (2.62 Å), revealing the contribution from two resonance forms, **A** (with a bimetallacyclopropene unit) and **B** (with the ruthenacarbyne coordinated to the copper center), as shown in fig. S13. The deviation from the least-squares plane through Cu1, Ru, and C1–C7 is only 0.023 Å, indicating that the Cu atom exists in the same plane as the five-membered metallabicycle. The Cu1–C1 bond length of 1.919(2) Å is within the range of typical Cu–C(aryl) bond lengths (1.849 to 2.020 Å). These results suggest that there is a strong interaction between the CuCl and Ru–C moieties and that resonance form **A** should be more important. To the best of our knowledge, complexes **4** represent the first ruthenium carbyne Cu(I) adducts, even though their osmium counterparts were obtained nearly 40 years ago (*40*, *41*).

Although a series of typical electrophiles, including MeI, MeOTf, EtOTf, Me_3OBF_4, and Et_3OBF_4, cannot react with ruthenium carbyne moieties of ruthenapentalynes **2**, we attempted to seek other electrophilic reactions. The metal-carbon triple bond of **2** could shift from the original ring to the other fused ring in the presence of acid. Such an extraordinary metal carbyne bond shift reaction has been observed only in osmium species (*21*). As shown in Fig. 3A, treatment of ruthenapentalyne **2b** with dichloroacetic acid at 0°C for 20 min formed new ruthenapentalyne **5**, which was characterized in situ. Ruthenapentalyne **5** is not stable in solution and persists only for 4 hours in the reaction mixture. Solution NMR spectra showed the expected chemical shift (13.03 ppm) for C^1H in ^{1}H NMR and the slightly up-field signal at 345.72 ppm in ^{13}C NMR for the carbyne carbon in comparison with that of the parent ruthenapentalyne **2b** (355.49 ppm for C^1). In addition, the HRMS shows an ion peak at mass/charge ratio (*m*/*z*) 1053.1892 corresponding to $[C_{63}H_{51}ClOP_3Ru]^+$. To understand the mechanistic aspects of the conversion of **2b** to **5**, we performed the experiments starting from deuterium-labeled acid. As shown in Fig. 3A, the isotopic-labeling experiment suggests that the hydrogen atom at the original carbyne carbon position in the product **5** comes from the acid proton. Thus, we think that the electrophilic attack of acid, on the carbyne carbon of **2a**, initiates the conversion reaction and produces a metal center 16e ruthenapentalene intermediate (Fig. 3B), owing to the ambiphilic reactivity of **2a**. The following elimination of proton from the C7 position of ruthenapentalene intermediate could yield the new ruthenapentalyne **5**. The proposed addition/elimination mechanism is similar to the metal carbyne bond shift reaction of osmapentalyne (*21*).

As suggested by the reactions of **2** with sodium thiophenoxide, CuCl, and acids ($Cl_2CHCOOH$ and CF_3COOD), ruthenapentalynes are ambiphilic. In general, metal carbyne complexes are either nucleophilic or electrophilic: Only a few of them can react with both nucleophiles and electrophiles (*12*, *42*, *43*). We assumed that the ambiphilic character

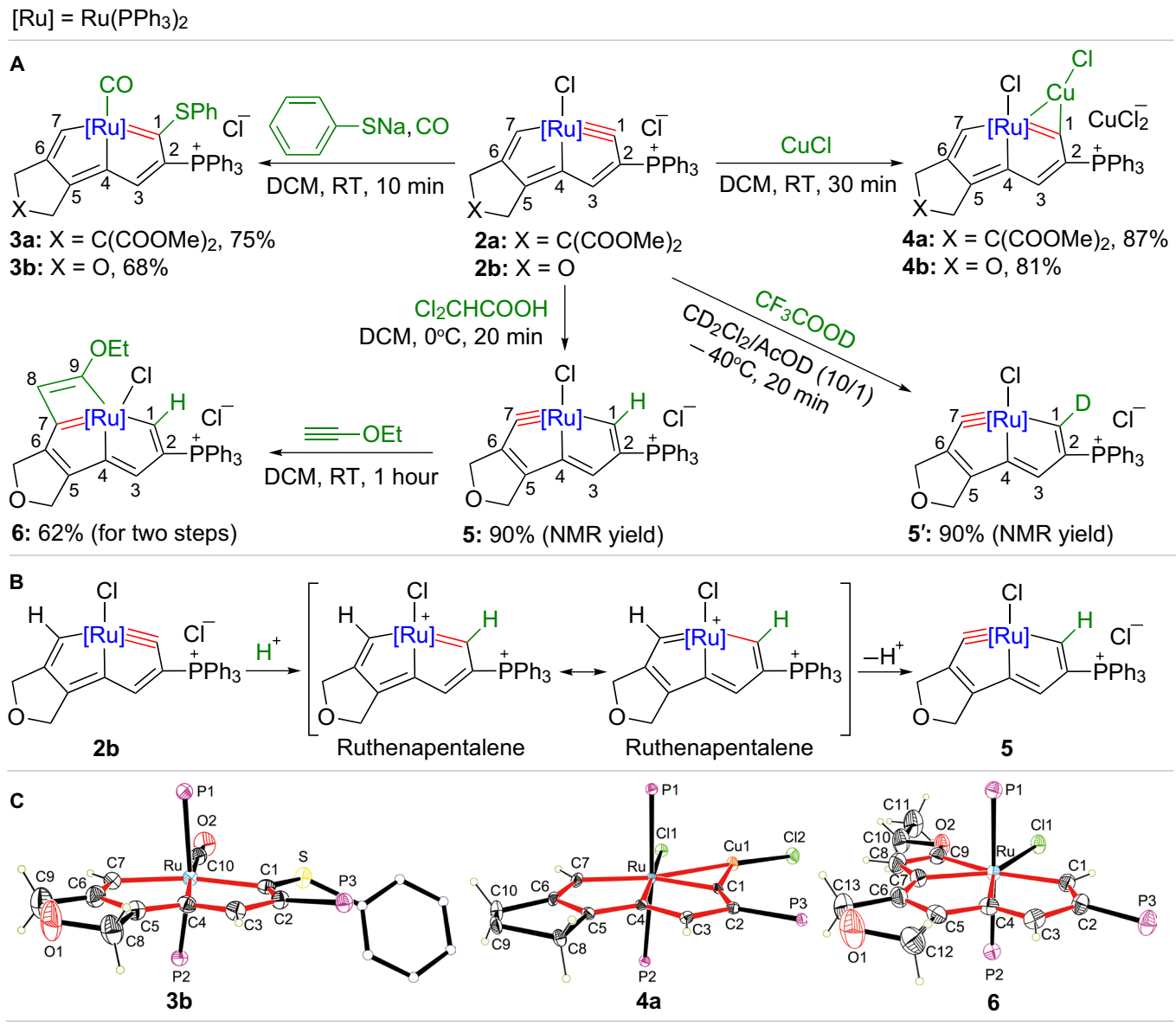

Fig. 3. Ambiphilic reactivity and [2 + 2] cycloaddition reaction of ruthenapentalynes. (**A**) Reactions of **2** with sodium thiophenoxide and CuCl, $Cl_2CHCOOH$, and CF_3COOD. (**B**) The proposed mechanism for the metal-carbon triple bond shift reaction of ruthenapentalyne **2b** in the presence of acid. (**C**) X-ray crystal structures of the cations of **3b**, **4a**, and **6** (the ellipsoids are drawn at the 50% probability level; phenyl groups of **3b**, **4a**, and **6** and ester groups of **4a** are omitted for clarity; the detailed structures are presented in figs. S2 to S4 for **3b**, **4a**, and **6**, respectively).

of **2** should be attributed to their extremely distorted Ru≡C–C moieties, which may result in a strong tendency to relieve the ring strain by transformation of the sp-hybridized carbyne carbons.

Since the thermal lability of **5** precluded its crystallographic characterization, we carried out the reactivity studies to further confirm its identity. Treatment of in situ prepared **5** with HC≡COEt in dichloromethane at RT for 1 hour afforded complex **6** (Fig. 3A). Complex **6** is stable enough to undergo NMR spectroscopy and single-crystal x-ray diffraction analysis. The core of **6** contains a four-membered ruthenacyclobutadiene ring (Fig. 3C), which is achieved via the [2 + 2] cycloaddition of the alkyne with the metal carbyne unit of **5**. Four Ru–C bonds are located in the equatorial plane in **4**, among which Ru–C1 [2.101(4) Å] and Ru–C7 [2.099(4) Å] are comparable and within the range of those of previous reported ruthenabenzenes (1.910 to 2.110 Å) (*20*, *36*), whereas the other two [Ru–C4, 2.143(4) Å; Ru–C9, 2.191(4) Å] are much longer. The carbon–carbon lengths of the metallatricycle fall within the range of 1.332(6) to 1.433(6) Å with slight alternation between C–C single and C=C double bonds.

The ruthenacyclobutadiene moiety of **6** supports the assignment of the location of the metal-carbon triple bond in ruthenapentalyne **5**. Although ruthenacyclobutadiene complexes have fascinated theoretical chemists (*44*, *45*), only one example has been achieved experimentally, which was prepared by tetramerization of phenylacetylide residues at ruthenium centers (*46*). For [2 + 2] cycloadditions of alkynes with metal carbyne complexes, there is only one previously reported example for the late–transition metal carbynes (*47*), although examples of early–transition metal carbyne complexes have been well documented (*48*–*50*). The formation of complex **6** represents the

first [2 + 2] cycloaddition reaction of a ruthenium carbyne complex with an alkyne.

Cascade cyclization reactions with ambident nucleophiles

Since the above investigation underlined the peculiarities of the metal carbyne moieties in ruthenapentalynes **2**, we next examined the reactions with ambident substrates to obtain more insight into their reactivities and properties. Accordingly, we first reacted **2** with cyanates. As shown in Fig. 4A, treatment of **2a** with excess NaOCN led to annulation complex **7**, which contained two molecules of the cyanate ion.

X-ray crystallographic analysis of **7** showed that the ruthenium center adopts a distorted pentagonal bipyramidal geometry with the equatorial plane vertexes occupied by four carbon atoms and one oxygen atom (Fig. 4B). The carbon-carbon bond lengths within the two five-membered metallacycles range from 1.353(6) to 1.452(6) Å. In the six-membered azametallacycle, the 1.285(6) Å C8–N1 and 1.313(6) Å C1–N2 distances are in the double-bond range and are significantly shorter than C9–N1 [1.391(6) Å] and C9–N2 [1.385(6) Å]. The exocyclic C9–O2 bond [1.239(6) Å] is a typical C=O double bond and shorter than C8–O1 [1.249(5) Å] within the three-membered ring. The Ru–C8 bond [2.040(4) Å] is the shortest Ru–C bond in **7**, which suggests a strong interaction between the metal centers and the OCN ligand. In comparison, the other three Ru–C bond lengths in **7** are 2.122(4), 2.087(4), and 2.141(4) Å for Ru–C1, Ru–C4, and Ru–C7, respectively. The structural parameters demonstrate an electron-localized structure of **7**, which can be represented by two resonance structures of **7A** and **7B** (Fig. 4A).

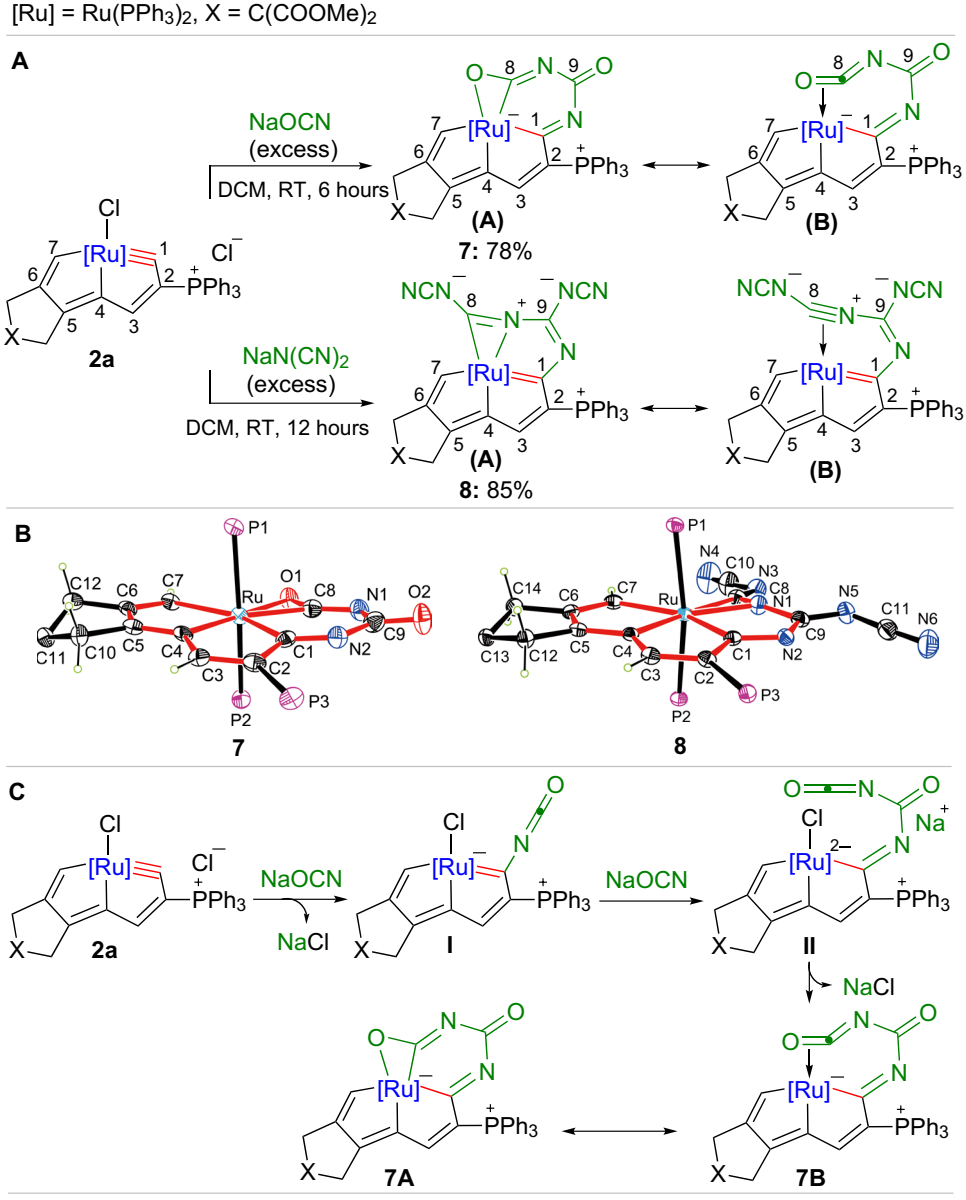

Fig. 4. Cascade cyclization reactions of ruthenapentalyne 2a. (**A**) Cascade cyclization reactions of **2a** with ambident nucleophiles. (**B**) X-ray molecular structures for complexes **7** and **8** (the ellipsoids are drawn at the 50% probability level; phenyl groups and ester groups are omitted for clarity; the detailed structures are presented in figs. S5 and S6 for **7** and **8**, respectively). (**C**) Proposed mechanism for the formation of **7**.

We outlined a proposed cascade cyclization mechanism in Fig. 4C. Initially, a nucleophilic attack of a cyanate ion at the carbyne carbon of **2a** would presumably lead to the formation of ruthenapentalene intermediate **I**, which can be further attacked by a second molecule of cyanate ion to yield intermediate **II**. The following coordination of the OCN group to the metal center, accompanied by the dissociation of the Cl group, could result in the final polycyclic complex **7**.

Sodium dicyanamide was shown to have a similar ambident ability to react with ruthenapentalynes **2** (Fig. 4A). We hypothesized that the access to annulation product **8** may proceed via a similar cascade cyclization reaction initiated by the nucleophilic attack of the $N(CN)_2$ ion (see fig. S8). X-ray diffraction analysis of **8** locates a five-membered and a three-membered azametallacycle fused with the ruthenapentalene skeleton (Fig. 4B). The Ru–N1 bond length is 2.021(3) Å, in accordance with an azaruthenacycle featuring Ru–N single bonds (*51*), whereas the Ru–C8 bond [2.213(3) Å] is slightly longer than the typical Ru–C bond length of a Ru–C=N moiety (1.962 to 2.177 Å). The carbon-nitrogen bond lengths of the five-membered azametallacycle [C1–N2, 1.338(4) Å; C9–N1, 1.386(4) Å; C9–N2, 1.362(4) Å] are similar to each other and lie between the typical lengths of carbon-nitrogen single and double bonds, but the carbon-nitrogen distance in the three-membered azametallacycle is 1.283(4) Å. Thus, complex **8** has a delocalized structure with contributions from the two resonance structures **8A** and **8B**, as shown in Fig. 4A.

The rich reactivities of ruthenapentalyne **2** allow access to a series of unusual polycyclic ruthenacycles, with aromatic stability and structural complexity. We summarized the ultraviolet-visible (UV-vis) absorption spectra of polycyclic ruthenacycles **2** to **4** and **6** to **8** in Fig. 5. All of them exhibit efficient absorption ranging from the UV-vis region. When the π-conjugated framework is extended, the characteristic energy absorption bands are relatively red-shifted. The broad absorption, unique structures, and remarkable stability could facilitate further application of these polycyclic ruthenacycles.

CONCLUSION

In summary, we have synthesized the first cyclic carbyne complexes with a second-row transition metal center, namely, ruthenapentalynes, by one-pot reactions of carbolongs with commercially available $RuCl_2(PPh_3)_3$. The carbyne carbon atom of the ruthenapentalyne shows a bond angle of only 130.2(3)°, which is greatly reduced compared to the previous record of the smallest angle within a second-row transition metal carbyne complex. Our experimental observations, together with theoretical calculations, revealed that the inherent aromaticity plays a key role in the stabilization of ruthenapentalynes. We demonstrated that because of the rich and unique reactivity, the ruthenapentalynes could serve as precursors to a family of ruthenacyclic complexes with diverse structural features and distinct properties. This work provides a valuable supplement to the previous paucity of transition metal carbyne complexes and may promote better understanding of the chemistry of cyclic metal carbyne complexes.

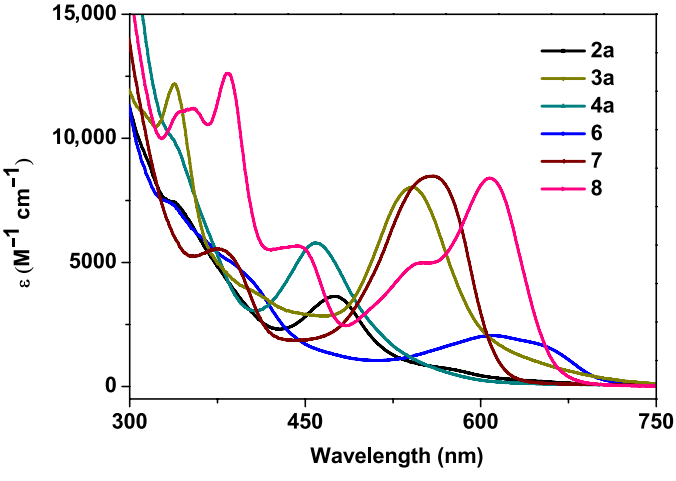

Fig. 5. UV-vis absorption spectra of 2a, 3a, 4a, 6, 7, and 8. Measured in CH_2Cl_2 at RT (1.0×10^{-4} M).

MATERIALS AND METHODS

All syntheses were performed under an inert atmosphere (N_2) using standard Schlenk techniques, unless otherwise stated. Solvents were distilled from sodium/benzophenone (hexane and diethyl ether) or calcium hydride (dichloromethane) under N_2 before use. The starting materials **1a** and **1b** were synthesized according to previously published procedures (*13*). Other reagents were used as received from commercial sources without further purification. Column chromatography was performed on silica gel (200 to 300 mesh) in air. NMR spectroscopy was performed using a Bruker Advance II 300 spectrometer, a Bruker Advance II 400 spectrometer, a Bruker Advance III 500 spectrometer, or a Bruker Ascend III 600 spectrometer at RT or 0°C. The ^1H and ^{13}C NMR chemical shifts (δ) are relative to tetramethylsilane, and the ^{31}P NMR chemical shifts are relative to 85% H_3PO_4. The absolute values of the coupling constants are given in hertz. The theoretical molecular ion peak was calculated by Compass Isotope Pattern software supplied by Bruker Company. HRMS was conducted using a Bruker Daltonics Apex Ultra 7.0 T FTMS instrument. EAs were performed on a vario EL III elemental analyzer. Absorption spectra were recorded on a Shimadzu UV2550 UV-vis spectrophotometer.

Representative syntheses are given below. Further details for the syntheses of complexes **2b**, **3b**, **4b**, and **5′** are given in the Supplementary Materials.

Complex 2a

A dichloromethane solution (5 ml) of carbolong **1a** (1.65 g, 6.29 mmol) was added slowly to a red solution of $RuCl_2(PPh_3)_3$ (3.54 g, 3.69 mmol) and PPh_3 (5.02 g, 19.1 mmol) in dichloromethane (150 ml). The reaction mixture was stirred at RT for 3 hours to yield a red solution. The solution was evaporated under vacuum to a volume of approximately 15 ml and then washed with hexane (3 × 200 ml) to afford a red solid. The solid was purified by flash chromatography on silica gel (eluent, 20:1 dichloromethane/methanol) to yield complex **2a** as a red solid. Yield: 2.89 g, 65%. ^1H NMR (600.1 MHz, CD_2Cl_2): δ 13.06 ppm (s, 1H, C^7H), 7.32 ppm [1H, C^3H, determined by heteronuclear single-quantum coherence (HSQC)], 7.00 to 7.78 ppm (45H of Ph and 1H of C^3H mentioned above), 3.63 ppm (s, 6H, $COOCH_3$), 2.94 ppm [t, ^5J(HP) = 3.82 Hz, 2H, $C^{10}H$], and 2.74 ppm (s, 2H, C^8H). ^{31}P NMR (242.9 MHz, CD_2Cl_2): δ 29.62 ppm [d, ^4J(PP) = 5.89 Hz, Ru*P*Ph_3] and 6.35 ppm [t, ^4J(PP) = 5.89 Hz, C*P*Ph_3]. ^{13}C NMR [150.9 MHz, CD_2Cl_2, plus ^{13}C DEPT-135, ^1H-^{13}C HSQC, ^1H-^{13}C heteronuclear multiple-bond correlation (HMBC)]: δ 355.69 ppm [dt, apparent q, ^2J(CP) = 14.92 Hz, ^2J(CP) = 14.92 Hz, C^1], 250.64 ppm (m, C^7), 189.01 ppm [dt, ^3J(CP) = 25.58 Hz, ^2J(CP) = 5.09 Hz, C^4], 179.74 ppm (s, C^5), 170.53 ppm (s, $COOCH_3$), 163.33 ppm

[t, ^3J(CP) = 3.62 Hz, C^6], 153.74 ppm [d, ^2J(CP) = 14.34 Hz, C^3], 126.98 to 134.52 ppm (Ph), 121.60 ppm [dt, ^1J(CP) = 92.66 Hz, ^3J(CP) = 3.51 Hz, C^2], 118.32 ppm [d, ^1J(CP) = 91.08 Hz, Ph], 62.90 ppm (s, C^9), 53.13 ppm (s, $COOCH_3$, obtained by ^{13}C DEPT-135), 37.80 ppm (s, C^8), and 36.10 ppm (s, C^{10}). Analysis calculated (Anal. calculated; %) for $C_{68}H_{57}Cl_2O_4P_3Ru$: C, 67.89; H, 4.78. Found: C, 67.60; H, 5.15. HRMS [electrospray ionization (ESI)]: *m/z* calculated for $[C_{68}H_{57}ClO_4P_3Ru]^+$, 1167.2212 $[M]^+$; found, 1167.2226.

Complex 3a

A mixture of **2a** (300 mg, 0.249 mmol) and NaSPh (99 mg, 0.75 mmol) in dichloromethane (10 ml) was stirred at RT for 10 min under an atmosphere of CO to yield a red solution. The solid was removed by filtration. The filtrate was evaporated under vacuum to approximately 2 ml and then purified by column chromatography on silica gel (eluent, 15:1 dichloromethane/methanol) to afford **3a** as a red solid. Yield: 244 mg, 75%. ^1H NMR (500.2 MHz, CD_2Cl_2): δ 10.87 ppm (s, 1H, C^7H), 7.83 ppm [d, ^3J(HP) = 5.45 Hz, 1H, C^3H], 7.04 to 7.68 ppm (45H, Ph), 6.88 ppm [t, ^3J(HH) = 7.40 Hz, 1H, Ph], 6.52 ppm [t, ^3J(HH) = 7.40 Hz, 2H, Ph], 5.99 ppm [d, ^3J(HH) = 7.40 Hz, 2H, Ph], 3.52 ppm (s, 6H, $COOCH_3$), 2.55 ppm (s, 2H, $C^{10}H$), and 2.09 ppm (s, 2H, C^8H). ^{31}P NMR (202.5 MHz, CD_2Cl_2): δ 36.79 ppm (s, Ru*P*Ph_3) and 7.28 ppm (s, C*P*Ph_3). ^{13}C NMR (125.8 MHz, CD_2Cl_2, plus ^{13}C-dept 135, ^1H-^{13}C HSQC, and ^1H-^{13}C HMBC): δ 249.56 ppm (br, C^1), 238.51 ppm [t, ^2J(CP) = 17.74 Hz, C^7], 203.96 ppm [t, ^2J(CP) = 15.06 Hz, Ru*C*O], 197.80 ppm [dt, ^3J(CP) = 27.45 Hz, ^2J(CP) = 7.71 Hz, C^4], 180.96 ppm (s, C^5), 171.71 ppm (s, *C*$OOCH_3$), 169.85 ppm (s, C^6), 161.86 ppm [d, ^2J(CP) = 24.53 Hz, C^3], 139.00 ppm (s, Ph), 128.29 to 135.33 ppm (Ph), 122.35 ppm [d, ^1J(CP) = 86.85 Hz, Ph], 121.97 ppm [d, ^1J(CP) = 59.36 Hz, C^2], 64.08 ppm (s, C^9), 53.32 ppm (s, $COOCH_3$), 38.38 ppm (s, C^{10}), and 37.62 ppm (s, C^8). Anal. calculated (%) for $C_{75}H_{62}ClO_5SP_3Ru$: C, 69.04; H, 4.79. Found: C, 68.92; H, 4.85. HRMS (ESI): *m/z* calculated for $[C_{75}H_{62}O_5P_3RuS]^+$, 1269.2589 $[M]^+$; found, 1269.2588.

Complex 4a

A mixture of complex **2a** (300 mg, 0.249 mmol) and CuCl (51 mg, 0.52 mmol) in dichloromethane (10 ml) was stirred for 30 min at RT to yield an orange solution. Excess CuCl was removed by filtration. The filtrate was evaporated under vacuum to approximately 3 ml and washed with diethyl ether (3 × 20 ml) to afford **4a** as an orange solid. Yield: 303 mg, 87%. ^1H NMR (400.1 MHz, CD_2Cl_2): δ 13.01 ppm [t, ^3J(HP) = 4.55 Hz, 1H, C^7H], 7.54 ppm (1H, C^3H, determined by HSQC), 7.04 to 7.81 ppm (45H of Ph and 1H of C^3H mentioned above), 3.64 ppm (s, 6H, $COOCH_3$), 2.86 ppm [t, ^5J(HP) = 3.76 Hz, 2H, $C^{10}H$], and 2.83 ppm (s, 2H, C^8H). ^{31}P NMR (161.9 MHz, CD_2Cl_2): δ 22.84 ppm [d, ^4J(PP) = 4.15 Hz, Ru*P*Ph_3] and 6.65 ppm [t, ^4J(PP) = 4.15 Hz, C*P*Ph_3]. ^{13}C NMR (100.6 MHz, CD_2Cl_2, plus ^{13}C-dept 135, ^1H-^{13}C HSQC, and ^1H-^{13}C HMBC): δ 325.76 ppm (br, C^1), 250.58 ppm [t, ^2J(CP) = 13.02 Hz, C^7], 194.40 ppm [dt, ^3J(CP) = 22.93 Hz, ^2J(CP) = 4.55 Hz, C^4], 184.57 ppm (s, C^5), 171.01 ppm (s, *C*$OOCH_3$), 166.52 ppm (s, C^6), 158.41 ppm [d, ^2J(CP) = 15.32 Hz, C^3], 128.58 to 135.45 ppm (Ph), 127.93 ppm [dt, ^1J(CP) = 87.05 Hz, ^3J(CP) = 3.81 Hz, C^2], 118.10 ppm [d, ^1J(CP) = 90.36 Hz, Ph], 63.98 ppm (s, C^9), 53.34 ppm (s, $COOCH_3$), 39.34 ppm (s, C^{10}), and 36.79 ppm (s, C^8). Anal. calculated (%) for $C_{68}H_{57}Cl_4Cu_2O_4P_3Ru$: C, 58.29; H, 4.10. Found: C, 58.22; H, 4.47. HRMS (ESI): *m/z* calculated for $[C_{68}H_{57}Cl_2CuO_4P_3Ru]^+$, 1267.1185 $[M]^+$; found, 1267.1187.

Complex 5

$Cl_2CHCOOH$ (58 μl, 0.703 mmol) was added to a solution of **2b** (300 mg, 0.275 mmol) in dichloromethane (15 ml). The reaction mixture was stirred at 0°C for 20 min to yield a red solution of **5** (in ca. 90% yield based on ^1H and ^{31}P NMR), which was characterized by in situ NMR and HRMS (ESI). ^1H NMR (600.1 MHz, CD_2Cl_2): δ 13.03 ppm [ddd, ^2J(HP) = 16.85 Hz, ^2J(HP) = 5.72 Hz, ^2J(HP) = 3.00 Hz, 1H, C^1H], 7.64 ppm (s, 1H, C^3H), 6.84 to 7.82 ppm (45H of Ph and 1H of C^3H mentioned above), 4.05 ppm (s, 2H, C^8H), and 3.55 ppm (s, 2H, C^9H). ^{31}P NMR (242.9 MHz, CD_2Cl_2): δ 32.53 ppm [d, ^4J(PP) = 4.93 Hz, Ru*P*Ph_3] and 12.16 ppm [t, ^4J(PP) = 4.93 Hz, C*P*Ph_3]. ^{13}C NMR (150.9 MHz, CD_2Cl_2, plus ^{13}C-dept 135, ^1H-^{13}C HSQC, and ^1H-^{13}C HMBC): δ 345.72 ppm (br, C^7), 249.98 ppm (br, C^1), 193.77 ppm (s, C^5), 187.73 ppm [dt, ^3J(CP) = 22.29 Hz, ^2J(CP) = 5.83 Hz, C^4], 157.59 ppm (s, C^6), 143.63 ppm [d, ^2J(CP) = 22.33 Hz, C^3], 127.07 to 134.34 ppm (Ph), 126.21 ppm [d, ^1J(CP) = 68.70 Hz, C^2], 117.73 ppm [d, ^1J(CP) = 88.44 Hz, Ph], 69.72 ppm (s, C^9), and 65.22 ppm (s, C^8). HRMS (ESI): *m/z* calculated for $[C_{63}H_{51}ClOP_3Ru]^+$, 1053.1893 $[M]^+$; found, 1053.1892.

Complex 6

$Cl_2CHCOOH$ (39 μl, 0.473 mmol) was added to a solution of **2b** (200 mg, 0.184 mmol) in dichloromethane (10 ml). The reaction mixture was stirred at 0°C for 20 min, and then HC≡COEt [71 μl (ω/ω = 50% *n*-hexane solution), 0.364 mmol] was added. The reaction mixture was further stirred for 1 hour at RT to yield a green solution. The solution was evaporated under vacuum to a volume of approximately 2 ml and washed with hexane (3 × 15 ml) to afford a green solid. The solid was purified by chromatography on silica gel (silicone; eluent, 20:1 dichloromethane/methanol) to yield complex **6** as a green solid. Yield: 132 mg, 62%. ^1H NMR (300.1 MHz, CD_2Cl_2): δ 12.40 ppm [dd, ^2J(HP) = 18.71 Hz, ^2J(HP) = 4.23 Hz, 1H, C^1H], 6.88 to 7.77 ppm (45H, Ph), 6.16 ppm (br, 1H, C^3H), 5.85 ppm [t, ^4J(HP) = 2.11 Hz, 1H, C^8H], 3.68 ppm [q, 2H, ^3J(HH) = 7.11 Hz, OCH_2CH_3], 3.52 ppm (s, 2H, $C^{12}H$), 3.43 ppm (s, 2H, $C^{13}H$), and 1.23 ppm [t, ^3J(HH) = 7.11 Hz, OCH_2CH_3]. ^{31}P NMR (121.5 MHz, CD_2Cl_2): δ 19.84 ppm [d, ^4J(PP) = 2.83 Hz, Ru*P*Ph_3] and 6.45 ppm [t, ^4J(PP) = 2.83 Hz, C*P*Ph_3]. ^{13}C NMR (75.5 MHz, CD_2Cl_2, plus ^{13}C-dept 135, ^1H-^{13}C HSQC, and ^1H-^{13}C HMBC): δ 253.15 ppm (br, C^1), 212.11 ppm (br, C^9), 204.92 ppm [t, ^2J(CP) = 8.92 Hz, C^7], 191.02 ppm [dt, ^3J(CP) = 28.00 Hz, ^2J(CP) = 9.16 Hz, C^4], 188.04 ppm (s, C^5), 151.34 ppm (s, C^6), 147.14 ppm [d, ^2J(CP) = 24.94 Hz, C^3], 126.77 to 133.90 ppm (Ph), 125.87 ppm [t, ^3J(CP) = 3.73 Hz, C^8], 121.36 ppm [d, ^1J(CP) = 71.91 Hz, C^2], 118.69 ppm [d, ^1J(CP) = 88.44 Hz, Ph], 68.74 ppm (s, C^{13}), 68.23 ppm (s, OCH_2CH_3), 65.11 ppm (s, C^{12}), and 12.96 ppm (s, OCH_2CH_3). Anal. calculated (%) for $C_{67}H_{57}Cl_2O_2P_3Ru$: C, 69.43; H, 4.96. Found: C, 69.07; H, 5.10. HRMS (ESI): *m/z* calculated for $[C_{67}H_{57}ClO_2P_3Ru]^+$, 1123.2313; found, 1123.2327.

Complex 7

A mixture of **2a** (300 mg, 0.249 mmol) and sodium cyanate (97 mg, 1.49 mmol) in dichloromethane (10 ml) was stirred for 6 hours at RT to yield a red solution. The solid was removed by filtration. The filtrate was evaporated under vacuum to approximately 2 ml and washed with diethyl ether (3 × 20 ml) to afford **7** as a red solid. Yield: 236 mg, 78%. ^1H NMR (600.1 MHz, CD_2Cl_2): δ 10.47 ppm (s, 1H, C^7H), 7.57 ppm (s, 1H, C^3H), 6.77 to 7.55 ppm (45H, Ph), 3.51 ppm (s, 6H, $COOCH_3$), 2.66 ppm (s, 2H, $C^{10}H$), and 2.42 ppm (s, 2H, $C^{12}H$). ^{31}P NMR (242.9 MHz, CD_2Cl_2): δ 29.89 ppm (s, Ru*P*Ph_3) and 12.24 ppm (s, C*P*Ph_3). ^{13}C

NMR (150.9 MHz, CD_2Cl_2, plus ^{13}C-dept 135, ^1H-^{13}C HSQC, and ^1H-^{13}C HMBC): δ 239.75 ppm (br, C^1), 207.71 ppm [t, ^2J(CP) = 14.89 Hz, C^7], 193.32 ppm [t, ^2J(CP) = 4.59 Hz, C^8], 181.46 ppm [dt, ^3J(CP) = 29.91 Hz, ^2J(CP) = 7.44 Hz, C^4], 173.36 ppm (s, C^9), 172.31 ppm (s, $COOCH_3$), 167.49 ppm (s, C^5), 162.04 ppm [d, ^2J(CP) = 19.22 Hz, C^3], 156.03 ppm (s, C^6), 127.19 to 134.67 ppm (Ph), 123.18 ppm [d, ^1J(CP) = 90.56 Hz, Ph], 122.91 ppm [d, ^1J(CP) = 75.83 Hz, C^2], 63.80 ppm (s, C^{11}), 52.61 ppm (s, $COOCH_3$), 38.10 ppm (s, C^{12}), and 37.71 ppm (s, C^{10}). Anal. calculated (%) for $C_{70}H_{57}N_2O_6P_3Ru$: N, 2.30; C, 69.13; H, 4.72. Found: N, 2.26; C, 68.81; H, 5.09. HRMS (ESI): *m/z* calculated for $[C_{70}H_{58}N_2O_6P_3Ru]^+$, 1217.2565 $[M + H]^+$; found, 1217.2568.

Complex 8

A mixture of complex **2a** (300 mg, 0.249 mmol) and sodium dicyanamide (133 mg, 1.49 mmol) in dichloromethane (10 ml) was stirred for 12 hours at RT to yield a navy blue solution. Excess sodium salt was removed by filtration. The filtrate was evaporated under vacuum to approximately 3 ml. Then, the residue was washed with diethyl ether (3 × 20 ml) to afford **8** as a green solid. Yield: 268 mg, 85%. ^1H NMR (400.1 MHz, CD_2Cl_2): δ 11.26 ppm (s, 1H, C^7H), 7.62 ppm (s, 1H, C^3H), 6.89 to 7.70 ppm (45H of Ph and 1H of C^3H mentioned above), 3.46 ppm (s, 6H, $COOCH_3$), 2.74 ppm (s, 2H, $C^{14}H$), and 2.62 ppm (s, 2H, $C^{12}H$). ^{31}P NMR (161.9 MHz MHz, CD_2Cl_2): δ 31.74 ppm (s, Ru*P*Ph_3) and 10.47 ppm (s, C*P*Ph_3). Unfortunately, the poor solubility of **8** prevented its ^{13}C NMR characterization. Anal. calculated (%) for $C_{72}H_{57}N_6O_4P_3Ru$: N, 6.65; C, 68.40; H, 4.54. Found: N, 7.01; C, 68.60; H, 4.42. HRMS (ESI): *m/z* calculated for $[C_{72}H_{58}N_6O_4P_3Ru]^+$, 1265.2790 $[M + H]^+$; found, 1265.2783.

SUPPLEMENTARY MATERIALS

Supplementary material for this article is available at http://advances.sciencemag.org/cgi/content/full/4/6/eaat0336/DC1

fig. S1. X-ray molecular structure for the cation of complex **2a**.
fig. S2. X-ray molecular structure for the cation of complex **3b**.
fig. S3. X-ray molecular structure for the cation of complex **4a**.
fig. S4. X-ray molecular structure for the cation of complex **6**.
fig. S5. X-ray molecular structure for complex **7**.
fig. S6. X-ray molecular structure for complex **8**.
fig. S7. Gibbs free-energy pathway for the DFT-calculated formation mechanism of complex **2a** at 298 K.
fig. S8. A plausible mechanism for the formation of complex **8**.
fig. S9. ASE evaluation of complex **3b**.
fig. S10. NICS evaluations of model complex **3b**′.
fig. S11. AICD plot of the model complex **3b**′ with an isosurface value of 0.03.
fig. S12. AICD plot of the model complex **2a**′ with an isosurface value of 0.03.
fig. S13. Resonance structures of complexes **4**.
fig. S14. Positive-ion ESI-MS spectrum of **[2a]**$^+$ $[C_{68}H_{57}ClO_4P_3Ru]^+$ measured in methanol.
fig. S15. Positive-ion ESI-MS spectrum of **[2b]**$^+$ $[C_{63}H_{51}ClOP_3Ru]^+$ measured in methanol.
fig. S16. Positive-ion ESI-MS spectrum of **[3a]**$^+$ $[C_{75}H_{62}O_5P_3RuS]^+$ measured in methanol.
fig. S17. Positive-ion ESI-MS spectrum of **[3b]**$^+$ $[C_{70}H_{56}O_2P_3RuS]^+$ measured in methanol.
fig. S18. Positive-ion ESI-MS spectrum of **[4a]**$^+$ $[C_{68}H_{57}Cl_2CuO_4P_3Ru]^+$ measured in methanol.
fig. S19. Positive-ion ESI-MS spectrum of **[4b]**$^+$ $[C_{63}H_{51}Cl_2CuOP_3Ru]^+$ measured in methanol.
fig. S20. Positive-ion ESI-MS spectrum of **[5]**$^+$ $[C_{63}H_{51}OClP_3Ru]^+$ measured in dichloromethane.
fig. S21. Positive-ion ESI-MS spectrum of **[5′]**$^+$ $[C_{63}H_{50}DOClP_3Ru]^+$ measured in dichloromethane.
fig. S22. Positive-ion ESI-MS spectrum of **[6]**$^+$ $[C_{67}H_{57}ClO_2P_3Ru]^+$ measured in methanol.
fig. S23. Positive-ion ESI-MS spectrum of **[7 + H]**$^+$ $[C_{70}H_{58}N_2O_6P_3Ru]^+$ measured in methanol.
fig. S24. Positive-ion ESI-MS spectrum of **[8 + H]**$^+$ $[C_{72}H_{58}N_6O_4P_3Ru]^+$ measured in methanol.
fig. S25. ^1H NMR spectrum (600.1 MHz) of complex **2a** in CD_2Cl_2 at RT.
fig. S26. ^{31}P NMR spectrum (242.9 MHz) of complex **2a** in CD_2Cl_2 at RT.
fig. S27. ^{13}C NMR spectrum (150.9 MHz) of complex **2a** in CD_2Cl_2 at RT.
fig. S28. ^1H NMR spectrum (300.1 MHz) of complex **2b** in CD_2Cl_2/CD_3OD (v/v = 3/1) at RT.
fig. S29. ^{31}P NMR spectrum (121.5 MHz) of complex **2b** in CD_2Cl_2/CD_3OD (v/v = 3/1) at RT.
fig. S30. ^{13}C NMR spectrum (75.5 MHz) of complex **2b** in CD_2Cl_2/CD_3OD (v/v = 3/1) at RT.
fig. S31. ^1H NMR spectrum (500.2 MHz, CD_2Cl_2) of complex **3a** at RT.
fig. S32. ^{31}P NMR spectrum (202.5 MHz, CD_2Cl_2) of complex **3a** at RT.
fig. S33. ^{13}C NMR spectrum (125.8 MHz, CD_2Cl_2) of complex **3a** at RT.
fig. S34. ^1H NMR spectrum (300.1 MHz, CD_2Cl_2) of complex **3b** at RT.
fig. S35. ^{31}P NMR spectrum (121.5 MHz, CD_2Cl_2) of complex **3b** at RT.
fig. S36. ^{13}C NMR spectrum (75.5 MHz, CD_2Cl_2) of complex **3b** at RT.
fig. S37. ^1H NMR spectrum (400.1 MHz, CD_2Cl_2) of complex **4a** at RT.
fig. S38. ^{31}P NMR spectrum (161.9 MHz, CD_2Cl_2) of complex **4a** at RT.
fig. S39. ^{13}C NMR spectrum (100.6 MHz, CD_2Cl_2) of complex **4a** at RT.
fig. S40. ^1H NMR spectrum (600.1 MHz, CD_2Cl_2) of complex **4b** at RT.
fig. S41. ^{31}P NMR spectrum (242.9 MHz, CD_2Cl_2) of complex **4b** at RT.
fig. S42. ^{13}C NMR spectrum (150.5 MHz, CD_2Cl_2) of complex **4b** at RT.
fig. S43. In situ ^1H NMR spectrum (600.1 MHz, CD_2Cl_2) of complex **5** at 0°C.
fig. S44. In situ ^{31}P NMR spectrum (242.9 MHz, CD_2Cl_2) of complex **5** at 0°C.
fig. S45. In situ ^{13}C NMR spectrum (150.9 MHz, CD_2Cl_2) of complex **5** at 0°C.
fig. S46. In situ ^1H NMR spectrum (500.2 MHz, CD_2Cl_2/CH_3COOD = 10/1) of complex **5′** at 0°C.
fig. S47. In situ ^{31}P NMR spectrum (202.5 MHz, CD_2Cl_2/CH_3COOD = 10/1) of complex **5′** at 0°C.
fig. S48. ^1H NMR spectrum (300.1 MHz, CD_2Cl_2) of complex **6** at RT.
fig. S49. ^{31}P NMR spectrum (121.5 MHz, CD_2Cl_2) of complex **6** at RT.
fig. S50. ^{13}C NMR spectrum (75.5 MHz, CD_2Cl_2) of complex **6** at RT.
fig. S51. ^1H NMR spectrum (600.1 MHz, CD_2Cl_2) of complex **7** at RT.
fig. S52. ^{31}P NMR spectrum (242.9 MHz, CD_2Cl_2) of complex **7** at RT.
fig. S53. ^{13}C NMR spectrum (150.9 MHz, CD_2Cl_2) of complex **7** at RT.
fig. S54. ^1H NMR spectrum (400.1 MHz, $CDCl_3$) of complex **8** at RT.
fig. S55. ^{31}P NMR spectrum (161.9 MHz, $CDCl_3$) of complex **8** at RT.
table S1. Crystal data and structure refinement for **2a**, **3b**, and **4a**.
table S2. Crystal data and structure refinement for **6**, **7**, and **8**.
table S3. Response to the questions raised in the checkCIF reports of complexes **4a**, **7**, and **8**.
table S4. Thermal decomposition data of complexes **2** to **4** and **6** to **8** in the solid state.
Supplementary Materials and Methods
data file S1. CIF files for complexes **2a**, **3b**, **4a**, **6**, **7**, and **8**.
data file S2. Cartesian coordinate–optimized structures for ASE, NICS, and AICD calculations.
data file S3. Cartesian coordinate–optimized structures for mechanism studies.
References (*52*–*60*)

REFERENCES AND NOTES

1. R. R. Schrock, High oxidation state multiple metal–carbon bonds. *Chem. Rev.* **102**, 145–180 (2002).
2. D. J. Mindiola, Oxidatively induced abstraction reactions. A synthetic approach to low-coordinate and reactive early transition metal complexes containing metal–ligand multiple bonds. *Acc. Chem. Res.* **39**, 813–821 (2006).
3. A. Fürstner, Alkyne metathesis on the rise. *Angew. Chem. Int. Ed. Engl.* **52**, 2794–2819 (2013).
4. R. H. Grubbs, A. G. Wenzel, D. J. O'Leary, E. Khosravi, Eds. *Handbook of Metathesis* (Wiley-VCH, ed. 2, 2015).
5. E. O. Fischer, G. Kreis, C. G. Kreiter, J. Müller, G. Huttner, H. Lorenz, *trans*-Halogeno[alkyl(aryl)carbyne]tetracarbonyl complexes of chromium, molybdenum, and tungsten —A new class of compounds having a transition metal-carbon triple bond. *Angew. Chem. Int. Ed. Engl.* **12**, 564–565 (1973).
6. T. B. Wen, Z. Y. Zhou, G. Jia, Synthesis and characterization of a metallabenzyne. *Angew. Chem. Int. Ed. Engl.* **40**, 1951–1954 (2001).
7. T. B. Wen, W. Y. Hung, H. H. Y. Sung, I. D. Williams, G. Jia, Syntheses of metallabenzynes from an allenylcarbene complex. *J. Am. Chem. Soc.* **127**, 2856–2857 (2005).
8. G. He, J. Zhu, W. Y. Hung, T. B. Wen, H. H.-Y. Sung, I. D. Williams, Z. Lin, G. Jia, A metallanaphthalyne complex from zinc reduction of a vinylcarbyne complex. *Angew. Chem. Int. Ed. Engl.* **46**, 9065–9068 (2007).
9. B. Liu, H. Xie, H. Wang, L. Wu, Q. Zhao, J. Chen, T. B. Wen, Z. Cao, H. Xia, Selective synthesis of osmanaphthalene and osmanaphthalyne by intramolecular C–H activation. *Angew. Chem. Int. Ed. Engl.* **48**, 5461–5464 (2009).
10. J. Chen, H. H. Y. Sung, I. D. Williams, Z. Lin, G. Jia, Synthesis and characterization of a rhenabenzyne complex. *Angew. Chem. Int. Ed. Engl.* **50**, 10675–10678 (2011).
11. T. Wang, H. Zhang, F. Han, R. Lin, Z. Lin, H. Xia, Synthesis and characterization of a metallapyridyne complex. *Angew. Chem. Int. Ed. Engl.* **51**, 9838–9841 (2012).
12. C. Zhu, S. Li, M. Luo, X. Zhou, Y. Niu, M. Lin, J. Zhu, Z. Cao, X. Lu, T. Wen, Z. Xie, P. v. R. Schleyer, H. Xia, Stabilization of anti-aromatic and strained five-membered rings with a transition metal. *Nat. Chem.* **5**, 698–703 (2013).
13. Q. Zhuo, J. Lin, Y. Hua, X. Zhou, Y. Shao, S. Chen, Z. Chen, J. Zhu, H. Zhang, H. Xia, Multiyne chains chelating osmium via three metal-carbon σ bonds. *Nat. Commun.* **8**, 1912 (2017).
14. J. Chen, K.-H. Lee, H. H. Y. Sung, I. D. Williams, Z. Lin, G. Jia, Synthesis and characterization of dirhenadehydro[12]annulenes. *Angew. Chem. Int. Ed. Engl.* **55**, 7194–7198 (2016).

15. J. P. Collman, L. S. Hegedus, J. R. Norton, R. G. Finke, *Principles and Application of Organotransition Metal Chemistry* (University Science Books, ed. 2, 1987), pp. 100.
16. J. R. Bleeke, Metallabenzenes. *Chem. Rev.* **101**, 1205–1228 (2001).
17. M. A. Iron, J. M. L. Martin, M. E. van der Boom, Metallabenzene versus Cp complex formation: A DFT investigation. *J. Am. Chem. Soc.* **125**, 13020–13021 (2003).
18. C. Anusha, S. De, P. Parameswaran, Ring contraction of six-membered metallabenzynes to five-membered metal–carbene complexes: A comparison with organic analogues. *Dalton Trans.* **42**, 14733–14741 (2013).
19. J. Fan, K. An, X. Wang, J. Zhu, Interconversion of metallanaphthalynes and indenylidene complexes: A DFT prediction. *Organometallics* **32**, 6271–6276 (2013).
20. H. Zhang, H. Xia, G. He, T. B. Wen, L. Gong, G. Jia, Synthesis and characterization of stable ruthenabenzenes. *Angew. Chem. Int. Ed. Engl.* **45**, 2920–2923 (2006).
21. C. Zhu, M. Luo, Q. Zhu, J. Zhu, P. v. R. Schleyer, J. I.-C. Wu, X. Lu, H. Xia, Planar möbius aromatic pentalenes incorporating 16 and 18 valence electron osmiums. *Nat. Commun.* **5**, 3265 (2014).
22. N. J. Beach, H. A. Jenkins, G. J. Spivak, Electrophilic attack on [Cp*Cl(PPh_3)Ru(CCHR)]: Carbyne formation vs. chloride abstraction. *Organometallics* **22**, 5179–5181 (2003).
23. M. Jiménez-Tenorio, M. C. Puerta, P. Valerga, M. A. Ortuño, G. Ujaque, A. Lledós, Counteranion-dependent reaction pathways in the protonation of cationic ruthenium–vinylidene complexes. *Organometallics* **33**, 2549–2560 (2014).
24. T. Wang, J. Zhu, F. Han, C. Zhou, H. Chen, H. Zhang, H. Xia, Synthesis of five-membered osmacycloallenes and conversion into six-membered osmacycloallenes. *Angew. Chem. Int. Ed. Engl.* **52**, 13361–13364 (2013).
25. V. Lavallo, C. A. Dyker, B. Donnadieu, G. Bertrand, Synthesis and ligand properties of stable five-membered-ring allenes containing only second-row elements. *Angew. Chem. Int. Ed. Engl.* **47**, 5411–5414 (2008).
26. M. Melaimi, P. Parameswaran, B. Donnadieu, G. Frenking, G. Bertrand, Synthesis and ligand properties of a persistent, all-carbon four-membered-ring allene. *Angew. Chem. Int. Ed. Engl.* **48**, 4792–4795 (2009).
27. J. A. Dean, N. A. Lange, *Lange's Handbook of Chemistry* (McGraw-Hill, 1999).
28. J. A. Pino-Chamorro, E. Bustelo, M. C. Puerta, P. Valerga, Allenylidene/alkenylcarbyne synthesis and reactivity in ruthenium complexes with monodentate phosphine ligands. *Organometallics* **28**, 1546–1557 (2009).
29. M. Baya, P. Crochet, M. A. Esteruelas, E. Gutiérrez-Puebla, A. M. López, J. Modrego, E. Oñate, N. Vela, Synthesis and characterization of hydride–alkynyl, allenylidene, carbyne, and functionalized-alkynyl complexes containing the $[Os(\eta^5\text{-}C_5H_5)(P^iPr_3)_2]^+$ fragment: The complex $[Os(\eta^5\text{-}C_5H_5)(C{=}C{=}CPh_2)(P^iPr_3)_2]PF_6$, a new type of allenylidene derivative from the reactivity point of view. *Organometallics* **19**, 2585–2596 (2000).
30. L. M. Caldwell, A. F. Hill, A. D. Rae, A. C. Willis, Alkynylselenolatoalkylidynes: $[Mo(\equiv CSeC\equiv CR)(CO)_2\{HB(pzMe_2)_3\}]$ (R = CMe_3, $SiMe_3$; $pzMe_2$ = 3,5-dimethylpyrazol-1-yl). *Organometallics* **27**, 341–345 (2008).
31. I. Fernández, G. Frenking, G. Merino, Aromaticity of metallabenzenes and related compounds. *Chem. Soc. Rev.* **44**, 6452–6463 (2015).
32. P. v. R. Schleyer, C. Maerker, A. Dransfeld, H. Jiao, N. J. R. van Eikema Hommes, Nucleus-independent chemical shifts: A simple and efficient aromaticity probe. *J. Am. Chem. Soc.* **118**, 6317–6318 (1996).
33. R. Herges, D. Geuenich, Delocalization of electrons in molecules. *J. Phys. Chem. A* **105**, 3214–3220 (2001).
34. B. J. Frogley, L. J. Wright, Recent advances in metallaaromatic chemistry. *Chem. - Eur. J.* **24**, 2025–2038 (2018).
35. J. Yang, W. M. Jones, J. K. Dixon, N. T. Allison, Detection of a ruthenabenzene, ruthenaphenoxide, and ruthenaphenanthrene oxide: The first metalla aromatics of a second-row transition metal. *J. Am. Chem. Soc.* **117**, 9776–9777 (1995).
36. G. R. Clark, T. R. O'Neale, W. R. Roper, D. M. Tonei, L. J. Wright, Stable cationic and neutral ruthenabenzenes. *Organometallics* **28**, 567–572 (2009).
37. J. Wei, W.-X. Zhang, Z. Xi, Dianions as formal oxidants: Synthesis and characterization of aromatic dilithionickeloles from 1,4-dilithio-1,3-butadienes and $[Ni(cod)_2]$. *Angew. Chem. Int. Ed. Engl.* **54**, 5999–6002 (2015).
38. Y. Zhang, J. Wei, Y. Chi, X. Zhang, W.-X. Zhang, Z. Xi, Spiro metalla-aromatics of Pd, Pt, and Rh: Synthesis and characterization. *J. Am. Chem. Soc.* **139**, 5039–5042 (2017).
39. J. Wei, W.-X. Zhang, Z. Xi, The aromatic dianion metalloles. *Chem. Sci.* **9**, 560–568 (2018).
40. G. R. Clark, C. M. Cochrane, W. R. Roper, L. J. Wright, The interaction of an osmium-carbon triple bond with copper(I), silver(I) and gold(I) to give mixed dimetallocyclopropene species and the structures of $Os(AgCl)(CR)Cl(CO)(PPh_3)_2$. *J. Organomet. Chem.* **199**, C35–C38 (1980).
41. M. A. Gallop, W. R. Roper, Carbene and carbyne complexes of ruthenium, osmium, and iridium. *Adv. Organomet. Chem.* **25**, 121–198 (1986).
42. H. F. Luecke, R. G. Bergman, Synthesis, structural characterization, and chemistry of a monomeric cationic iridium carbyne complex. *J. Am. Chem. Soc.* **120**, 11008–11009 (1998).
43. L. M. Caldwell, A. F. Hill, A. C. Willis, Selenoaroyl complexes of molybdenum. *Chem. Commun.* **0**, 2615–2617 (2005).
44. Z. Lin, M. B. Hall, Stabilities of metallacyclobutadiene and metalatetrahedrane complexes. *Organometallics* **13**, 2878–2884 (1994).
45. J. Wu, Y. Hao, K. An, J. Zhu, Unexpected higher stabilisation of two classical antiaromatic frameworks with a ruthenium fragment compared to the osmium counterpart: Origin probed by DFT calculations. *Chem. Commun.* **52**, 272–275 (2016).
46. M. I. Bruce, G. A. Koutsantonis, M. J. Liddell, E. R. T. Tiekink, Cyclopentadienyl-ruthenium and -osmium chemistry: XXXVI. Oligomerisation of phenylacetylide residues on ruthenium. Crystal structures of $\{Ru(PPh_3)(\eta\text{-}C_5H_5)\}_2(\mu\text{-}C_8Ph_4)$ and $\{Ru(PPh_3)(\eta\text{-}C_5H_5)\}_2\{\mu\text{-}C_{10}Ph_4(C_6H_4)\}$. *J. Organomet. Chem.* **420**, 253–269 (1991).
47. C. Zhu, Y. Yang, M. Luo, C. Yang, J. Wu, L. Chen, G. Liu, T. Wen, J. Zhu, H. Xia, Stabilizing two classical antiaromatic frameworks: Demonstration of photoacoustic imaging and the photothermal effect in metalla-aromatics. *Angew. Chem. Int. Ed. Engl.* **54**, 6181–6185 (2015).
48. S. F. Pedersen, R. R. Schrock, M. R. Churchill, H. J. Wasserman, Reaction of tungsten(VI) alkylidyne complexes with acetylenes to give tungstenacyclobutadiene and cyclopentadienyl complexes. *J. Am. Chem. Soc.* **104**, 6808–6809 (1982).
49. S. Beer, C. G. Hrib, P. G. Jones, K. Brandhorst, J. Grunenberg, M. Tamm, Efficient room-temperature alkyne metathesis with well-defined imidazolin-2-iminato tungsten alkylidyne complexes. *Angew. Chem. Int. Ed. Engl.* **46**, 8890–8894 (2007).
50. D. P. Estes, C. P. Gordon, A. Fedorov, W.-C. Liao, H. Ehrhorn, C. Bittner, M. L. Zier, D. Bockfeld, K. W. Chan, O. Eisenstein, C. Raynaud, M. Tamm, C. Copéret, Molecular and silica-supported molybdenum alkyne metathesis catalysts: Influence of electronics and dynamics on activity revealed by kinetics, solid-state NMR, and chemical shift analysis. *J. Am. Chem. Soc.* **139**, 17597–17607 (2017).
51. J. F. Hartwig, R. G. Bergman, R. A. Andersen, Structure, synthesis, and chemistry of ruthenium complex $(PMe_3)_4Ru(\eta^2\text{-benzyne})$. Reactions with arenes, alkenes, and heteroatom-containing organic compounds. Synthesis and structure of a monomeric hydroxide complex. *J. Am. Chem. Soc.* **113**, 3404–3418 (1991).
52. P. J. Hay, W. R. Wadt, *Ab initio* effective core potentials for molecular calculations. Potentials for K to Au including the outermost core orbitals. *J. Chem. Phys.* **82**, 299–310 (1985).
53. C. Lee, W. Yang, R. G. Parr, Development of the Colle-Salvetti correlation-energy formula into a functional of the electron density. *Phys. Rev. B* **37**, 785–789 (1988).
54. B. Miehlich, A. Savin, H. Stoll, H. Preuss, Results obtained with the correlation energy density functionals of Becke and Lee, Yang and Parr. *Chem. Phys. Lett.* **157**, 200–206 (1989).
55. A. D. Becke, Density-functional thermochemistry. III. The role of exact exchange. *J. Chem. Phys.* **98**, 5648–5652 (1993).
56. C. Peng, P. Y. Ayala, H. B. Schlegel, M. J. Frisch, Using redundant internal coordinates to optimize equilibrium geometries and transition states. *J. Comput. Chem.* **17**, 49–56 (1996).
57. J. Tao, J. P. Perdew, V. N. Staroverov, G. E. Scuseria, Climbing the density functional ladder: Nonempirical meta–generalized gradient approximation designed for molecules and solids. *Phys. Rev. Lett.* **91**, 146401 (2003).
58. G. Scalmani, M. J. Frisch, Continuous surface charge polarizable continuum models of solvation. I. General formalism. *J. Chem. Phys.* **132**, 114110 (2010).
59. S. Huzinaga, J. Andzelm, M. Klobukowski, E. Radzio-Andzelm, Y. Sakai, H. Tatewaki, *Gaussian Basis Sets for Molecular Calculations* (Elsevier, 1984).
60. M. J. Frisch, G. W. Trucks, H. B. Schlegel, G. E. Scuseria, M. A. Robb, J. R. Cheeseman, G. Scalmani, V. Barone, B. Mennucci, G. A. Petersson, H. Nakatsuji, M. Caricato, X. Li, H. P. Hratchian, A. F. Izmaylov, J. Bloino, G. Zheng, J. L. Sonnenberg, M. Hada, M. Ehara, K. Toyota, R. Fukuda, J. Hasegawa, M. Ishida, T. Nakajima, Y. Honda, O. Kitao, H. Nakai, T. Vreven, J. A. Montgomery Jr., J. E. Peralta, F. Ogliaro, M. Bearpark, J. J. Heyd, E. Brothers, K. N. Kudin, V. N. Staroverov, R. Kobayashi, J. Normand, K. Raghavachari, A. Rendell, J. C. Burant, S. S. Iyengar, J. Tomasi, M. Cossi, N. Rega, J. M. Millam, M. Klene, J. E. Knox, J. B. Cross, V. Bakken, C. Adamo, J. Jaramillo, R. Gomperts, R. E. Stratmann, O. Yazyev, A. J. Austin, R. Cammi, C. Pomelli, J. W. Ochterski, R. L. Martin, K. Morokuma, V. G. Zakrzewski, G. A. Voth, P. Salvador, J. J. Dannenberg, S. Dapprich, A. D. Daniels, O. Farkas, J. B. Foresman, J. V. Ortiz, J. Cioslowski, D. J. Fox, *Gaussian 09, Revision B.01* (Gaussian Inc., 2009).

Acknowledgments

Funding: This research was supported by the National Key R&D Program of China (2017YFA0204902) and the National Natural Science Foundation of China (nos. 21490573, 21332002, and 21561162001). **Author contributions:** H.X. conceived this project. Q.Z., H.K., and X.L. performed synthesis experiments and recorded NMR data. Q.Z., Z.C., X.Z., and J.L. solved x-ray structures. H.X., H.Z., Q.Z., and H.K. analyzed experimental data. H.Z. conceived the theoretical work. Y.H. conducted theoretical computations. K.Z. measured UV-vis absorption spectra. Q.Z., H.X., H.Z., and X.Z. drafted the paper. All authors discussed the results and contributed to the preparation of the final manuscript. **Competing interests:** H.X., Q.Z., J.L., X.Z., K.Z., and H.Z. are inventors on a published patent related to this work filed by Xiamen University (no. CN106543232A, filed 29 March 2017). Q.Z., H.Z., X.Z., J.L., Z.C., and H.X. are inventors on a published patent related to this work filed by Xiamen University

(no. CN106279100A, filed 4 January 2017).The authors declare no other competing interests.
Data and materials availability: All data needed to evaluate the conclusions in the paper are present in the paper and/or the Supplementary Materials. Additional data related to this paper may be requested from the authors. Crystal data of **2a**, **3b**, **4a**, **6**, **7**, and **8** are available from the Cambridge Crystallographic Data Centre under reference numbers CCDC-1506332, CCDC-1580872, CCDC-1580879, CCDC-1580868, CCDC-1580893, and CCDC-1580880 (www.ccdc.cam.ac.uk/data_request/cif).

Submitted 19 January 2018
Accepted 10 May 2018
Published 22 June 2018
10.1126/sciadv.aat0336

Citation: Q. Zhuo, H. Zhang, Y. Hua, H. Kang, X. Zhou, X. Lin, Z. Chen, J. Lin, K. Zhuo, H. Xia, Constraint of a ruthenium-carbon triple bond to a five-membered ring. *Sci. Adv.* **4**, eaat0336 (2018).

Science Advances

Constraint of a ruthenium-carbon triple bond to a five-membered ring

Qingde Zhuo, Hong Zhang, Yuhui Hua, Huijun Kang, Xiaoxi Zhou, Xinlei Lin, Zhixin Chen, Jianfeng Lin, Kaiyue Zhuo and Haiping Xia

Sci Adv **4** (6), eaat0336.
DOI: 10.1126/sciadv.aat0336